LAWRENCE
LIVERMORE
NATIONAL
LABORATORY

LLNL-JRNL-642413

The Effects of Mesoscale Confinement in Pu Clusters and Isolated Particles

M. V. Ryzhkov, A. Mirmelstein, B. Delley, S. W. Yu, B. W. Chung, J. G. Tobin

August 15, 2013

Journal of Electron Spectroscopy and Related Phenomena

Disclaimer

The Effects of Mesoscale Confinement in Pu Clusters and Isolated Particles

M.V. Ryzhkov[1*], A. Mirmelstein[2], B. Delley[3] , S.-W. Yu[4], B.W. Chung[4], J.G. Tobin[4]

[1]Institute of Solid State Chemistry, Ural Division of the Russian Academy of Science, Ekaterinburg,Russia,
[2]Department of Experimental Physics, Russian Federal Nuclear Center, E.I.Zababakhin Institute of Technical Physics (VNIITF), Snezhinsk, Russia,
[3]Paul Scherrer Institut WHGA 123, CH-5232, Villigen PSI, Switzerland
[4]Lawrence Livermore National Laboratory, Livermore, CA, USA 94550,
*Corresponding author: ryz@ihim.uran.ru

Abstract

Calculations of the electronic structure of Pu crystal clusters and isolated particles formed by a finite number of atoms, have been performed in terms of the fully relativistic discrete variational method, using two types of atomic wave functions incorporated into the RDV code. The density of states results for the central atoms of the finite-size Pu systems as well as the calculated 4f core level energy schemes, for the clusters of different size and structure have been compared to the relevant experimental spectra obtained by synchrotron-radiation-based photoelectron spectroscopy. The robust result of our investigation is the observation of systematic average electronic structure evolution from atomic to bulk behavior through the cluster/nanoparticle regime. The effects of mesoscale confinement established in the present work impose certain limitation for the electronic structure of bulk plutonium and can be useful for the interpretation of Pu photoelectron spectra.

Key words: electronic structure; scalar and fully relativistic calculations; atomic configurations; photoelectron spectroscopy

The Effects of Mesoscale Confinement in Pu Clusters and Isolated Particles

1. Introduction

Quantum-chemical electronic structure calculations of finite-size actinide systems, which are based on the cluster approach, allow us to follow the development of atomic wave functions when going from an isolated atom to a solid. From consideration of the size dependence of the results obtained it may be possible to get substantial and new insight into the nature of the electronic structure of bulk actinide materials. Recently we performed electronic structure calculations of the plutonium clusters formed by 19 (Pu_{19}) and 79 (Pu_{79}) atoms using the fully relativistic discrete variational (RDV) method [1]. The calculated partial and total density of states (DOS) for Pu_{79} clusters were compared to spectroscopic data produced in the experimental investigations of bulk systems, including Photoelectron Spectroscopy (PES) [2,3]. This direct comparison, which shows good agreement for Pu5f, Pu6d, $Pu6p_{1/2}$, and $Pu6p_{3/2}$ manifolds, between the experimental data and the DOS calculated for the central atom of the Pu_{79} cluster, is very important because of two reasons. First, it demonstrates the validity of the cluster approach, supporting the assertion that the central atom of cluster should converge to a bulk-like state. Second, it demonstrates that the cluster calculations may represent a useful avenue to address unresolved questions within the field of actinide electronic structure.

While the central atom manifests a bulk-like condition, the size dependence of the result obtained in Ref. [1] follows from the consideration of site-averaged properties, including weighetd contributions from each type of atom in the moiety. For example, the Pu5f, Pu6d, Pu7s, and Pu7p average occupations for four Pu systems, namely, a Pu atom, a Pu dimer (diatomic molecule Pu_2), and two Pu clusters, Pu_{19} and Pu_{79} were calculated. Particularly, we found that the Pu5f population n_f decreases monotonically from the Pu atom (n_f =6) to the Pu dimer (n_f=5.85) to the Pu19 cluster (n_f=5.66) to the Pu79 cluster (n_f=5.33), and, being plotted as a function of the

cube root of the number of atoms in the system, produces a linear relationship. The observation of this linear dependence supports the contention of the validity of the cluster approach used in Ref.1. If the occupancies were not dependent upon size in such a fundamental and direct way, it is unlikely that a linear dependence would be observed. From the results obtained in [1] it is evident that with the increase of system size the net transfer of electronic density is from the 5f and 7s into the 6d and 7p states, in agreement with the concept put forward earlier by Cooper et al., that hybridization between the relativistic 5f (large spin-orbit, tending toward a jj limit) and the 6d, 7s and 7p "valence" electrons, is the key to bonding in the actinides [4-6].

Though the manifestation of size effects in our cluster calculations is rather well proved in our previous study [1], one should keep in mind two important circumstances. The first is connected with the boundary conditions. In Ref. [1] we considered clusters that were part of an infinitely repeating matrix [7-9], with only a boundary between adjacent clusters. (See section 2 for details.) The second point is related to the choice of basis wave functions (atomic orbitals) firmware into the RDV code. The RDV method utilizes natural atomic basis orbitals, and this is the basic feature of the method. However, the choice of basis functions is arbitrary to some extent. In Ref. [1] the standard "extended" basis set was used which includes "virtual" (unoccupied) atomic states $Pu7p_{1/2}$ and $Pu7p_{3/2}$ in addition to the occupied atomic orbitals. This may lead to some artificial results such as negative DOS and negative populations of these orbitals.

To elucidate the limitations resulting from the boundary conditions and basis set used earlier [1], in the present paper we repeat the RDV calculations for crystal Pu_{19} and Pu_{79} clusters using a modified set of atomic orbitals, calculate electronic structure for a large crystal cluster formed by 201 Pu atoms, and performed the RDV study of isolated (or free-standing) Pu_{19} and Pu_{79} nanoparticles. The calculated results are compared to the relevant experimental

spectroscopic data, including valence band and 4f core level PES. Finally, we discuss the electronic configurations of Pu atoms on the surface and in the center for both crystalline cluster and isolated particles of different size and show that the main trend in the variation of electronic structure of the Pu clusters as a function of size depends neither on boundary conditions nor on the basis set used in the RDV calculations.

2. Systems under study, computational and experimental methods

In the crystal lattice of δ-Pu (fcc structure, Fm3m space group, lattice parameter a = 4.637 Å) each metal site has twelve nearest neighbors and six next nearest neighbors. As a first step of electronic structure investigation of Pu clusters, we consider the simple cluster model of this crystal consisting of only nineteen plutonium atoms. The structure of this cluster is illustrated in Fig. 1. The next steps to investigate the influence of crystal boundaries on the electron density redistribution in a finite-size cluster is consideration of the greater size fragments of the δ-Pu-like crystal lattice formed by 79 (Pu_{79}) and 201 (Pu_{201}) atoms (Fig.1).

In the bulk limit, a finite fragment of the crystal lattice can be used as a model for the description of some properties of infinite crystal, using the original scheme of "Extended Cluster" boundary conditions [8,9]. In this model, the crystal fragment under study consists of two parts: the internal main part (or the "core" of the cluster) and the outer part (or the "shell"). The outer part usually includes the atoms from 1 to 10 coordination spheres surrounding the "core". During the self-consistency procedure, the electron densities and the potential of the atoms in the "shell" are replaced by the corresponding values obtained for the crystallographically equivalent centers of the cluster "core". To introduce the long-range component of the surrounding-crystal potential, the extended cluster is embedded into a pseudopotential formed by the outer crystal lattice, which includes a few thousands of centers. Coulomb and exchange-correlation potentials of these

pseudo-centers are also substituted by the corresponding values obtained for the equivalent atoms in the internal part of the cluster [10]. This pseudopotential modeling of the long-range crystal potential usually improves convergence and becomes very important in the calculations of compounds with noticeable charges on atoms, such as oxides and fluorides. Obviously, it is impossible to develop an ideal model for the boundary conditions, which will completely simulate the influence of infinite crystal. (In this hypothetical case, the results for small and large fragments must be the same.). In our scheme the size effect certainly takes place [1], however, as mentioned above the atomic positions correspond to those in fcc crystal and do not depend on the particular boundary conditions. In the last decade, a set of calculations showed that this approach can be used successfully for the description of photoelectron spectra of the solid actinide compounds [11-13].

Since in the case of small Pu_{19} cluster we are interested in the interaction of the central atom with its nearest neighbors, the cluster "core" includes only one atom in the center of cluster (labeled below as Pu1). The twelve plutonium sites of the next coordination sphere (Pu2) and the six next nearest neighbors (Pu3) form the "shell" and, during self-consistency, their electron densities and potentials were kept equivalent to those of Pu1. This Pu_{19} cluster can serve as a "core" of the new fragment containing 79 atoms, i.e. the Pu_{79} cluster (Fig. 1). However, in this case, there are no any restrictions with respect to the electronic characteristics of Pu2 and Pu3 centers during calculations. All three types of atoms in the "core" are considered simply as nonequivalent atoms in a molecule. The "shell" around the cluster "core" is formed by the atoms of the three next coordination spheres (24Pu4, 12Pu5, and 24Pu6) providing the complete set of nearest neighbors for the atoms of a "core". During self-consistency, the electron densities and potentials of Pu4, Pu5, and Pu6 were kept equivalent to those of Pu1. Finally, in the cluster

containing 201 atoms the "core" also includes nineteen plutonium atoms (Pu1, 12Pu2, and 6Pu3) (Fig. 1), while the "shell" is formed by the atoms of the next nine coordination spheres (24Pu4, 12Pu5, 24Pu6, 6Pu7, 48Pu8, 8Pu9, 12Pu10, 24Pu11 and 24Pu12) providing better "bulk like environment" for all atoms in the "core" (Fig. 1). During self-consistency, the electron densities and potentials of Pu4 –Pu12 atoms were kept equivalent to those of Pu1.

Consideration of isolated (free-standing) particles represents the other, and may be the most direct route to investigate the development of electronic structure of the systems under study as a function of size. Respectively, in the present work we are also interested in the electronic structure of isolated Pu_{19} and Pu_{79} nanoparticles, which can be generated from the crystal, for example, due to crystal destruction. It is evident, that the geometry of the isolated cluster should differ from that of the crystal fragment due the relaxation to a new equilibrium structure. To model the relaxation of atomic positions, the geometry optimization of the Pu_{19} and Pu_{79} cluster was performed using $DMol^3$ method [14,15] in the scalar relativistic approximation [16,17] with double numerical atomic basis set, including additional polarization functions ("dnp"). The calculations were performed in the generalized gradient approximation (GGA) for the exchange-correlation potential in the "PBE" form [18]. Optimization of the particle structure proceeded until the variation of the value of maximum energy gradients did not become less than 0.001 atomic units. The global orbital cutoff was 8.0 Å.

Calculations of the electronic structure of crystal clusters and isolated nanoparticles were performed by the fully Relativistic Discrete Variational method (RDV) [19,20]. The RDV method is based on the solution of the Dirac-Slater equation for four-component relativistic wave functions transforming according to irreducible representations of the double point groups. As in

ref. 1, in the present calculations the "normal" Dirac theory is used, and the spin-polarization is neglected.

As mentioned above, our version of the RDV method utilizes the basis sets of four-component numerical atomic orbitals (AOs) obtained as solution of the Dirac-Slater equation for the isolated neutral atoms. The use of such "most natural basis orbitals" and the absence of any M-T approximation to potential and electron density allow one to obtain the occupation numbers of atomic orbitals (AOs), which are more realistic than those calculated by the electron distribution on the partial waves in the band structure approach.

Thus, the use of natural basis orbitals is the basic feature of the RDV method. The simplest (or "minimal") basis set, which can be used in RDV calculation includes the AOs completely or partially occupied in a neutral atom. This minimal basis set usually provides the correct description of the valence and deeper states in the cluster. However, for the investigation of vacant states and for more variation freedom one should use the "extended" basis sets including "virtual" (unoccupied) atomic orbitals, which also can be obtained by the solution of the Dirac-Slater equation for the isolated neutral atoms. In our previous work [1] for the RDV calculations of Pu_{19} and Pu_{79} crystal clusters the "extended" basis included $7p_{1/2}$ and $7p_{3/2}$ functions in addition to occupied AOs. The same basis set is used in the present paper to calculate the electronic structure of isolated Pu_{19} particle.

However, these "virtual" AOs are usually considerably delocalized and overlap with the electron density of atoms belonging to distant coordination spheres, leading to some artificial results such as negative partial densities of states (DOS) and occupation numbers for 7p states. (See Table 1 and Figures 2 and 3 in Ref 1.) The latter feature of these AOs makes the inclusion of 7p wave functions to the basis quite questionable. To minimize this problem the basis function

are usually truncated during calculations of isolated atoms (typical R_{cut} values are close to 8 - 10 Å). Hence, the present work includes the electronic structure calculations for Pu_{19}, Pu_{79}, and Pu_{201} crystal clusters and Pu_{19} and Pu_{79} free-standing particles using the "truncated" basis set. However, this procedure can lead to some deformation of "real" basis functions, such as 6d or 7s. For this reason it is useful to compare the results obtained with standard and truncated sets of basis functions. Such a comparison is also performed in the present work.

Moreover, the results of the cluster calculations will be compared to experimental photoelectron spectroscopic (PES) data. The synchrotron-radiation-based PES measurements were performed mainly at the Advanced Light Source, as described elsewhere [2,3].

3. Results and discussion

3.1 Structure of isolated Pu_{19} and Pu_{79} particles

In the crystal lattice of δ-Pu all atoms are symmetrically equivalent and the Pu - Pu bond lengths equal 3.28 Å. As in ref. 1, the crystal clusters considered here have the same structural parameters. To obtain the structure of isolated Pu_{19} particles the structural relaxation procedure was performed (see Section 2) leading to a new equilibrium state. Due to the structure relaxation, the binding energy (which is sometimes called the "total bond energy" or the "atomization energy") of the Pu_{19} cluster decreased from -21.40 to -21.65 eV. As expected, the structure of nanoparticle became more compact, the distances between central Pu1 atom and its twelve nearest neighbors Pu2 decreased from 3.28 Å to 3.13 Å. The distances between the cluster center and the second neighbors Pu3 also decreased from 4.64 Å to 4.53 Å, and the Pu2 - Pu3 bond lengths shrunk from 3.28 Å to 3.20 Å. In general, the shape of isolated particle remained similar to that of cluster in crystal (Fig. 1).

A similar procedure was applied to the Pu_{79} crystal cluster to obtain new equilibrium structure of isolated Pu_{79} particle. Due to relaxation, the binding energy of this cluster decreased from -138.03 to -140.40 eV (much more than in the case of Pu_{19}). The geometry of nanoparticle became also more compact, the distances between central atom Pu1 and Pu2 decreased from 3.28 Å to 3.18 Å (much less as compared to Pu_{19}). The distances between cluster center and Pu3 decreased from 4.64 Å to 4.37 Å, the Pu2 - Pu3 bond lengths shrunk from 3.28 Å to 3.09 Å. The shifts of atoms forming the "shell" of particle were not monotonic. The decrease in the Pu1-Pu4 distance equals 0.24 Å, between Pu1 and Pu5 equals 0.15 Å, and between Pu1 and Pu6 equals 0.35 Å (the highest value obtained due to geometry optimization). Nevertheless, as in the case of Pu^{19} nanoparticle, the visual shape of Pu_{79} isolated particle remained similar to that of the cluster in crystal.

The optimized atomic positions for the isolated Pu_{19} and Pu_{79} particles were used to calculate the electronic structure of these systems by the fully relativistic RDV method. Note, that during self-consistency we did not use any corrections to electron density and potentials of outer atoms in the particles.

3.2. Electronic structure of Pu_{19} and Pu_{79} clusters: crystal fragments vs. isolated particles

In this section we compare the results of RDV electronic structure calculations for crystal clusters and isolated particles obtained with "truncated" basis set. As a whole, the total and partial densities of states for the central Pu1 atom for both Pu_{19} crystal cluster and Pu_{19} particle are rather similar (Fig.2), although there are some differences in band width and peak intensities. The crystal cluster is characterized by more narrow 6p, 6d, and 5f bands. Small difference is obtained also in some details of the line shape for the most delocalized 7s and 7p bands. Variations in peak intensities are connected with diverse contributions to DOS coming from different cluster atoms.

For example, the Highest Occupied Molecular Orbital (HOMO) of Pu_{19} crystal cluster contains 41% of 5f AOs of the Pu2 sites and 24% of the Pu3 5f states with admixtures of Pu2 6d (16%) and Pu3 7s (11%) states. There are no noticeable contributions to HOMO from any states of central Pu1 atom. On the contrary, the Lowest Unoccupied Molecular Orbital (LUMO) contains 16% of Pu1 5f AOs, although the main contributions also come from Pu2 5f (31%) and Pu3 5f (23%) states.

In the isolated Pu_{19} particle HOMO contains almost equal contributions (34%) from 5f atomic orbitals of Pu2 and Pu3 sites with admixtures of 6d AOs of Pu2 and Pu3 (13% and 7% respectively). The contribution to HOMO from 5f AOs of Pu1 is about 3%. On the other hand, there are no significant contributions from atomic orbitals of Pu1 to LUMO, and the main contributions come from Pu3 5f (55%) and Pu2 5f (17%) states.

Figure 3 shows the total and partial densities of states for the central Pu1 atom in Pu_{79} crystal cluster and isolated particle formed by the same number of Pu atoms. It is immediately seen that DOS for these two systems became more similar than in the case of Pu_{19} systems. The main difference between DOS in Pu_{79} cluster and Pu_{79} particle is observed for the most delocalized 7s and 7p bands.

The HOMO in Pu_{79} cluster contains only 1% of 5f AOs of the Pu1 site, 23% of 5f Pu2 and Pu3 AOs, and 48% of the 5f states from surface atoms (Pu4, Pu5, and Pu6) with admixtures of 16% of 6d AOs of the same sites, i.e., the main contributions to HOMO come from the atoms of cluster “shell”. The LUMO of Pu_{79} cluster has no contributions from the central atom wave functions. As well as in the case of HOMO, the main contributions to LUMO of Pu_{79} cluster results from 5f (47%) and 6d (16%) states of surface atoms.

The main contributions (65%) to HOMO of Pu_{79} isolated particle come from 5f atomic

orbitals of Pu4, Pu5, and Pu6 sites with admixtures of 6d AOs of these surface atoms (10%). The contribution to HOMO from 5f AOs of internal Pu2 and Pu3 atoms is about 17%. Similarly, there are no noticeable contributions from atomic orbitals of Pu1 to LUMO, and the main contributions result from 5f AOs of atoms located in the outer part of this particle, i.e., Pu4 (21%), Pu5 (13%), and Pu6 (34%).

In any finite size object, there is a variation of potential at the positions of symmetrically non-equivalent atoms within the cluster. As a result, the energy positions of valence and core levels could differ for central and surface atoms in the cluster as well as in the isolated particles. The partial densities of 6s states for three types of non-equivalent atoms in the Pu_{19} cluster and the Pu_{19} particle obtained in the present work, are shown in Fig. 4. The heights of three 6s peaks directly reflects the number of corresponding atoms in the cluster, namely, one central atom Pu1 (solid line, the lowest DOS in Fig. 4), twelve Pu2 atoms (broken line, the highest peak), and six Pu3 atoms (dashed line, intermediate DOS). As seen, there is almost no difference between 6s DOS for the crystal fragment and isolated particle of the same size. In both cases the binding energy increases when going from the cluster center to its surface. The only difference is the slightly less total splitting between three 6s lines in the Pu_{19} particle (0.58 eV) than in the Pu_{19} crystal fragment (0.65 eV).

In the Pu_{79} system one can distinguish internal Pu1, Pu2, and Pu3 sites with complete nearest neighborhood and Pu4, Pu5, and Pu6 positions, which can be considered as surface sites, partially or completely. The partial 6s DOS for the Pu_{79} crystal fragment and the Pu_{79} isolated particle are shown in Fig. 5. The contributions from all six non-equivalent Pu sites are indicated. In the crystal fragment the total splitting of 6s band decreases as compared to the Pu_{19} crystal cluster (0.52 eV vs. 0.65 eV, respectively), while the inverse variation is found for the isolated

particles, where the total splitting increases from 0.58 to 0.69 eV when going from Pu_{19} to Pu_{79} particles. It is interesting to note, that in the Pu_{79} crystal fragment the bottom of 6s band (high binding energy) is formed mainly by the outer sites of cluster, Pu4 (80%) and Pu5 (15%), while the top of this band (lower binding energy) originates from the contributions of internal atoms, Pu2 (15%) and Pu3 (80%). Similar structure of 6s band is found in the case of both Pu_{19} systems (see Fig. 4 for a comparison). Opposite, in the Pu_{79} particle we see that the bottom of 6s band is formed by the internal sites, Pu2 (70%) and Pu3 (25%), while the main contributions to the top of this band comes from outer atoms, Pu4 (80%) and Pu6 (17%).

We also investigated the core level states of 4f character for Pu_{19} and Pu_{79} crystal fragments and free-standing particles (Fig. 6). In Pu_{19} crystal cluster the bottoms (high binding energy) of both $4f_{5/2}$ and $4f_{7/2}$ sub-bands are formed by the outer Pu3 sites, while the central Pu1 atom contributes to the top of these sub-bands. This is the same "order of contributions" with respect to their binding energy as found for the 6s states in both Pu_{19} systems (crystal fragment and isolated particle). As for the Pu_{19} particle, the "inverse" 4f peaks order takes place, i.e. the bottoms and tops of $4f_{5/2}$ and $4f_{7/2}$ sub-bands are formed by the central Pu1 atom and the outer Pu3 sites, respectively. This is similar to the case of 6s band in the Pu_{79} particle. The total splitting of each $4f_{5/2}$ and $4f_{7/2}$ sub-band increases from 0.64 eV in the Pu_{19} crystal fragment to 0.83 eV in the Pu_{19} particle.

The energy schemes of $4f_{5/2}$ and $4f_{7/2}$ core levels for both Pu_{79} systems are also shown in Fig. 6. Here the situation is more complicated[1]. In the crystal fragment both central (Pu2 and Pu3) and outer (Pu4 and Pu5) sites contribute to the DOS at the bottom of 4f sub-bands. However, the tops of these sub-bands are formed mainly by the sites from the central part (Pu2) of the cluster. Therefore, in spite of the above complication, up to some extent the 4f energy scheme in

Pu_{79} crystal cluster can be characterized by the "direct order" of atomic contributions, similar to that in the Pu_{19} systems. In the Pu_{79} particle the "inverse" order of contributions to 4f DOS is found, similar to the case of 6s states in this system. Namely, the bottoms of $4f_{5/2}$ and $4f_{7/2}$ sub-bands are formed by the internal sites (Pu1, Pu2, Pu3) while the tops are formed by the outer sites (P4 and Pu6).

Now we can compare the calculated 4f DOS with the experimental results produced in the core level photoemission spectroscopic (PES) measurements from a large crystallite δ-Pu sample and a polycrystalline α-Pu sample [2]. First of all, note different energy scales for the theoretical and experimental 4f spectra in Figure 6. The calculated binding energy for $4f_{5/2}$ and $4f_{7/2}$ sub-bands are about -422 and – 409 eV, respectively, being less than the corresponding experimental values. However the calculated value of spin-orbit splitting ~ 13 eV, almost the same for all the Pu_{19} and Pu_{79} systems under study, is found to be in excellent agreement with experimentally observed value. Of course, the calculated DOS cannot reproduce details of the experimental PES data, since our cluster calculations do not account for the 4f PE final state with a hole in the 4f shall. Particularly, our calculations cannot reproduce a broad satellite feature resulting from a poorly screened 4f hole in Pu. [21, 22] Excluding this feature, we see a rather good agreement between experimental and calculated 4f DOS. The best agreement is seen for the 4f DOS of Pu_{79} crystal cluster which is calculated using the "Extended Cluster" scheme.

3.3. Size dependence of DOS in plutonium clusters

The largest Pu cluster considered in the present work contains 201 Pu atoms. As expected, in this case the RDV calculations appear to be extremely time consuming. Because of this the geometry optimization for isolated Pu_{201} particle even in the scalar relativistic approach could not be performed at reasonable time. Hence, only calculations for the Pu_{201} crystal cluster with fcc δ-

Pu-like structure (Fig. 1) were carried out. Although the final convergence for valence electronic states and especially for unoccupied bands was not achieved, the obtained energy positions of core levels were calculated with an acceptable accuracy. The total and partial densities of states obtained for the central Pu1 atom in the Pu_{201} crystal fragment are shown in Fig. 8. Calculations are performed using truncated basis set. The comparison of DOS for Pu_{79} (Fig. 3) and Pu_{201} clusters reveals similar positions, widths and even the shapes of internal $6p_{1/2}$ and $6p_{3/2}$ bands.

The 6d DOS undergoes also substantial transformation. While the left edges of these bands are located at the same energy ~ 3 eV below the Fermi level, within the unoccupied region the shape of DOS changes significantly. Particularly, the four-peak structure between 20 and 25 eV, well visible in the Pu_{79} cluster DOS, practically disappears in the Pu_{201} DOS. The 5f DOS of Pu_{201} cluster displays less pronounced peak structure as compared that of Pu_{79} crystal fragment. However, in both clusters the occupied part of valence band is formed by the hybridized 5f – 6d orbitals and the states at the bottom of this band are mainly of the 6d character. The most pronounced difference is found for the delocalized 7p bands. The increase in cluster size induces the increased contributions of 7p atomic orbitals to DOS at the energies above 25 eV as well as rather strong shift of the 7p band upper from 27 eV in Pu_{79} to 38 eV in Pu_{201}. As in the Pu_{79} crystal cluster, the Pu_{201} 7p DOS shows a negligible negative contribution.

Because the number of non-equivalent atoms in Pu_{201} is two times higher than in the Pu_{79} cluster, we do not illustrate the structures of 4f and 6s bands by the partial densities of states. However, we can say that the bottoms of core level 6s and 4f bands in this large crystal cluster are formed by the outer cluster atoms while the main contributions to the tops of these bands come from the internal part of the cluster. By the other words, here we have the “direct order of contributions, the same as in the crystal fragments of the smaller sizes, while for the both Pu_{19}

and Pu_{79} isolated particles the "inverse order" was obtained (excluding the 6s bands of Pu_{19} particle). Therefore, it seems likely that the energy schemes of core level bands depend mainly on the boundary conditions rather than on the cluster size.

Figure 9 sums up the evolution of total Pu1 DOS calculated with truncated basis for all the crystal clusters and free-standing particles under consideration. The number of atoms in the system increases from the bottom to the top. The upper panel of Fig. 9 shows the electronic density of states of metallic plutonium obtained at photon energy 125 eV (on resonance) by Resonance Photoemission Spectroscopy (RESPES) technique [2]. The Pu sample was alpha with a delta-like reconstruction on the surface. It should be emphasized that no energy scale adjustments were applied to calculated or experimental data shown in Fig. 9. As seen, there is a remarkable agreement between the simulated occupied DOS for 6p and 5f/6d manifolds and the relevant experimental features. Moreover, beautiful convergence of the calculated 5f/6d Pu1 DOS to the bulk limit given by the experimental data is evident when going from the small Pu_{19} systems to the large Pu_{201} crystal cluster.

In Section 3.5 we will continue to discuss the size dependence of electronic structure of Pu clusters in terms of state occupation.

3.4. Effect of wave function truncation

To understand the effect of wave function truncation we compare the density of states calculated for Pu_{19} crystal fragment and Pu_{19} isolated particle using both extended and truncated basis sets. The total and partial DOS for Pu_{19} systems obtained with standard extended basis are shown in Fig. 7. Comparison of DOS for the crystal fragments (left sides of Fig. 7 and Fig. 2) shows certain variations. First of all, the use of truncated functions (R_{cut} = 8 Å) decreases significantly the negative 7s and $7p_{3/2}$ DOS but do not remove completely this unphysical effect.

Also, truncated basis shifts the 7s and 7p states towards the lower energy and leads to hybridization between delocalized 7p and "deep" 6p orbitals. Subtle differences are found also for the 5f, 6d (different intensities above the Fermi level), and 6p (inverse peak intensities) states.

Similar sorts of variations are found for the Pu_{19} particle (for a comparison see the right sides of Figures 2 and 7). The use of truncated basis suppresses significantly negative 7s and 7p DOS and removes strong contributions of these states at high energies above the Fermi level. Band shape of $6p_{3/2}$ states also changes. At the same time only subtle difference is observed for 6d and 5f DOS.

In the case of Pu_{79} crystal clusters the main effects of basis cutoff also consist in the strong but not complete suppression of negative 7s and 7p DOS (see Fig. 3 of Ref.[1] and Fig. 3 of this article for a comparison), increased admixture of delocalized 7p orbitals in the occupied region of valence band as well as to weak hybridization between 7p and 6p orbitals.

Additional aspects of the wave function cutoff are also discussed in the next Section.

3.5. Size dependence of level occupation

One of the crucial issues to resolve the enigma of metallic plutonium is to establish the precise value of 5f count in all plutonium allotropes. The alpha- and delta- phases are the most intriguing from this point of view. Recently, a fairly close consensus concerning 5f count in the metallic plutonium metal has been achieved, within an error of ± 0.2 electrons. This consensus includes both both theoretical [23, 24] and experimental [3, 25] determinations, producing a bulk value of 5f occupancy that is about 5.2-5.4. However, the experimental results still point towards a lower value of 5f occupation, nearer to but greater than 5 [3], possibly 5.2 to 5.3 [25]. Moreover, there is increasing evidence for the mixed-valence nature of plutonium metal, the ground-state properties of which involve fluctuations between at least three integer-valence electronic

configurations with five ($5f^5$), four ($5f^4$), and six ($5f^6$) electrons in Pu 5f shell [22-26]. However, the pathway from an individual Pu atom to the fluctuating ground state of bulk plutonium is not yet understood in detail, nor the microscopic quantum mechanisms that are driving this crossover. This pathway problem can be illustrated by the inconsistent interpretations of photoemission spectra from plutonium ultrathin films experimentally determined by Havela et al. [21]. The interpretations were suggested by van der Laan and Tagichi [22], from the one hand, and Kolorenc et al. [27], from the other. We already discussed this contradiction in last section of Ref. [1], where we argued clearly that the results of our cluster calculations agree with the results of Kolorenc et al. and contradict with those of van der Laan and Tagichi. However, our quantum-chemical calculations, as any *ab initio* electronic structure calculations, are not free of certain technical approximations such as boundary conditions and/or a choice of basis functions. In the previous section of this paper we discussed the influence of conditions of our study on the density of states for the central Pu1 atom in the cluster. Clearly, the effects are not negligible, but we do claim that neither boundary conditions nor the basis functions used can shake the general trend of Pu electronic structure evolution as a function of size which follows from our RDV cluster investigations. Since the state occupations are the key point in plutonium problem, below the variation of Pu electronic structure vs. size is discussed in terms of electronic configuration (or state occupation) of Pu ions which form crystal fragments and free-standing Pu particles.

Tables 1 and 2 contain a summary of the state occupations for the Pu_{19} and Pu_{79} crystal clusters and isolated particles, including a breakdown by sites. These values are obtained by Mulliken population analysis [28]. As in Ref. 1, we calculated a weighted average of the occupations for each object studied, multiplying each configuration's population by the number of atoms of that site type, summing over all sites types and then dividing by the total number of

atoms in the cluster. The result is the average configuration, which has the reassuring result that the total number of electrons in the valence range is eight. Of course, eight is the number of electrons that should be on Pu, outside of the Radon-like atomic-center with 86 electrons.

We start with a discussion of the state occupations, given in Tables 1and 2, from the effect of basis truncation. From Table 1, for the case of Pu_{19} crystal cluster the truncation suppresses the negative 7p state occupation almost completely. We already observed this effect while discussing the Pu1 DOS in the previous sections of this paper. The 7s state occupation decreases for Pu1 and Pu2 sites but increases slightly for Pu3 sites when truncation is applied. 6d state occupation reveals opposite behavior, i.e. the occupation decreases for Pu1 and Pu2 sites and increases for Pu3 sites as a result of truncation. 5f population decreases for the central Pu1 atoms and increases for the sites of the Pu_{19} cluster "shell". In the average, 5f and 7s populations grow and 6d goes down as a result of truncation. Note, that variations of the state populations reflect the changes of DOS.

For the case of Pu_{19} isolated particle, the effect of wave function truncation is slightly different. All the 7p populations become positive. Population of 7s states increases as a result of truncation while 5f state population decreases as well as 6d population for Pu1 and Pu2 sites. Average 5f population decreases (opposite to the case of Pu_{19} crystal cluster), 6d population also decreases (as well in the case of crystal cluster), and 7s population grows (as well as in the case of crystal fragment). From Table 1, the most important conclusion is as follows: the 5f and 7s populations decrease when going from the cluster "shell" to the cluster center while 6d population has the inverse behavior. Therefore, this trend is independent of boundary conditions (fcc structure with fixed atomic positions vs. free-standing particle with equilibrium structure obtained by the relaxation procedure) and the type of the basis used (extended basis set vs.

truncated basis with R_{cut} = 8 Å). Note, the basis truncation differently affects the average 5f population in Pu_{19} crystal cluster and Pu_{19} isolated particle, namely, this value increases in the former and goes down in the latter.

In the both the Pu_{79} crystal fragment and isolated particle states occupations display non-monotonic behavior when going from the surface to the cluster center, with the extrema near Pu3 or P4 sites (Table 2). It is important, however, that this behavior is found for all the cases listed in Table 2, i.e. it depends neither on the boundary conditions nor on the type of the used basis. Also, similar to the case Pu_{19} crystal cluster, the basis truncation increases the 5f population and decreases the occupation of 6d states.

It should be emphasized that the unphysical effect of the negative 7p and 7s populations is completely suppressed if the isolated particles are treated using the truncated basis sets. This circumstance speaks in favor of truncated basis for the RDV cluster calculations.

Following Reference 1, in order to illustrate the dependence of state occupation as function of cluster size, we use the cube root of the number of atoms N in the system as the proper abscissa. Figure 10 displays the size dependence of the average state occupations for an isolated Pu atom [29], Pu dimer [30], crystal fragments formed by 19, 79, and 201 atoms, as well as for the isolated particles consisting of 19 and 79 atoms. The results in Fig. 10 include those obtained with the truncated basis set. As mentioned above, in the case of large Pu_{201} crystal cluster the perfect convergence for the valence states is still not achieved, however, the average occupations appears to be quite stable during several iterations: $5f^{5.39}6d^{1.83}7s^{0.65}7p^{0.13}$. These occupations are shown in the left part of Fig. 10. The isolated Pu_{201} particle was not available because of extreme computing-time consumption.

The comparison of the left part of Fig.10 with the Fig. 5 from Ref. 1 reveals that the basis

truncation does not change all the tendencies in the behavior of the average state occupations as a function of size found in [1], though the occupation values are different for two basis sets (see Table 1 and 2). These tendencies are: the Pu5f state population decreases almost linearly as a function of cluster size. The highly delocalized 7p states seem to correlate with the 5f states. After an initial jump between the atom and dimer, the occupancy drops in a fairly linear fashion with size. On the other hand, the 6d and 7s state occupancies are almost mirror images of each other, without a simple linear relationship for either. This empirical connection suggests the transfer of electronic density from the 7s into the 6d, corresponding to the development of bonding within the Pu structures.

Basically, the same character of the state occupations vs. cluster size dependencies also holds for the isolated Pu particles. The only qualitative difference is that in the case of isolated particles the average occupations of 5f, 7s, and 7p states indicate a sign of saturation to some limiting values already for the number of atoms in the system N = 79.

4. Summary and Conclusions

Calculations of electronic structure of Pu crystal clusters and isolated particle have been performed by the fully relativistic discrete variational method using two types of the atomic wave functions incorporated into the RDV code. The DOS results for the central atoms of Pu systems as well as the calculated 4f core level energy schemes for the clusters of different size and structure have been compared to the relevant experimental spectra obtained by photoemission spectroscopy. The robust result of our investigation manifests itself in the evolution from atomic to bulk behavior through the cluster/nanoparticle regime. In our initial approach, published in [1], we considered the clusters that were the part of an infinitely repeated matrix and we used the standard functions of atomic orbitals including the highly delocalized 7p orbitals, i.e. the

extended basis set. We argued in Ref. [1] that despite the infinite nature of the matrix, the clusters "feel" the boundary and that the effect of the negative 7p densities can be neglected. To address the concerns associated with these shortcomings, in the present paper two very important avenues of attack have been pursued. First, we used truncated functions for cluster calculations. Second, we calculated the electronic structure behavior for isolated nano-clusters of the finite sizes. As a result, we got the same trend for all of these systems independently of calculation conditions. The effects of measoscale confinement established in the present work impose certain limitation for the electronic structure of bulk plutonium, such as interlinked behavior of the 5f, 6d, 7s, and 7p states, and can be useful for the correct interpretation of Pu photoemission spectra.

Acknowledgements

Lawrence Livermore National Laboratory is operated by Lawrence Livermore National Security, LLC, for the U.S. Department of Energy, National Nuclear Security Administration under Contract No. DE-AC52- 07NA27344. JGT and SWY were supported by the DOE Office of Science, Office of Basic Energy Science, Division of Materials Science and Engineering. Work at the RAS and VNIITF was supported in part by Contract B601122 between LLNL and VNIITF. The Advanced Light Source (ALS) in Berkeley and the Stanford Synchrotron Radiation Laboratory are supported by the DOE Office of Science, Office of Basic Energy Science.

References

[1] M. V. Ryzhkov, A. Mirmelstein, S.-W. Yu, B. W. Chung, and J. G. Tobin, Int. J. Quantum Chem. **113**, 1957 (2013).

[2] J. G. Tobin, B. W. Chung, R. K. Schulze, J. Terry, J. D. Farr, D. K. Shuh, K. Heinzelman, E. Rotenberg, G. D. Waddill, and G. van der Laan, Phys. Rev. B**68**, 155109 (2003).

[3] J.G. Tobin, P. Söderlind, A. Landa, K.T. Moore, A.J. Schwartz, B.W. Chung, M.A. Wall, J.M. Wills, R.G. Haire, and A.L. Kutepov, J. Phys. Cond. Matter **20**, 125204 (2008).

[4] B. R. Cooper, R. Siemann, D. Yang, P. Thamyaballi and A. Banerjea, "Hybridization-Induce Anisotropy in Cerium and Actinide Systems, in *Handbook on the Physics and Chemistry of the Actinides,* edited by A. J. Freeman and G. H. Lander (Elsevier Science, Amsterdam, 1985), Vol. 2.

[5] B. R. Cooper, P. Thayamballi, J. C. Spirlet, W. Mueller, and O. Vogt, Phys. Rev. Lett. 51, 2418 (1983).

[6] Y. G. Hao, O. Eriksson, G. W. Fernando, B. R. Cooper, Phys. Rev. B **43**, 9467, (1991).

[7] M.V. Ryzhkov, A.Ya. Kupryazhkin, J. Nucl. Materials **384**, 226 (2009).

[8] M.V. Ryzhkov, N.I. Medvedeva, V.A. Gubanov, Physica Scripta **48**, 629 (1993).

[9] M.V. Ryzhkov, N.I. Medvedeva, V.A. Gubanov, J. Phys. Chem. Solids **56**, 1231 (1995).

[10] D.E. Ellis, G.A. Benesh, E. Byrom, Phys. Rev.B. **20**, 1198 (1979).

[11] A.Yu. Teterin, Yu.A. Teterin, K.I. Maslakov, A.D. Panov, M.V. Ryzhkov, L. Vukcevic, Phys. Rev. B **74**, 045101 (2006).

[12] M.V. Ryzhkov, A.Yu. Teterin, Yu.A. Teterin, Int. J. Quant. Chem. **110**, 2697 (2010).

[13] Yu.A. Teterin, K.I. Maslakov, A.Yu. Teterin, K.E. Ivanov, M.V. Ryzhkov, V.G. Petrov, D.A. Enina, S.N. Kalmykov, Phys. Rev. B **87**, 145108 (2013).

[14] B. Delley, J. Chem. Phys. **92**, 508 (1990).

[15] B. Delley, J. Chem. Phys. **113**, 7756 (2000).

[16] D.D. Koelling, B.N. Harmon, J. Phys. C: Solid State Phys. **10**, 3107 (1977).

[17] M. Douglas, N.M. Kroll, Acta Phys. **83**, 89 (1974).

[18] J.P. Perdew, S. Burke, M. Ernzerhof, Phys. Rev. Lett. **77**, 3865 (1996).

[19] A. Rosen, D.E. Ellis, J. Chem. Phys. **62**, 3039 (1975).

[20] H. Adachi, Technol. Rep. Osaka Univ. 27, 569 (1977)

[21] L. Havela, T. Gouder, F. Wastin, and J. Rebizant, Phys. Rev. B **65**, 235118 (2002)

[22] G. van der Laan and M. Taguchi, Phys. Rev. B **82**, 045114 (2010)

[23] J.H. Shim, K. Haule, and G. Kotliar, Nature **446**, 513 (2007).

[24] E. Gorelov, J. Kolorenč, T. Wehling, H. Hafermann, A. B. Shick, A. N. Rubtsov, A. Landa, A. K. McMahan, V. I. Anisimov, M. I. Katsnelson, and A. I. Lichtenstein, Phys. Rev. B **82**, 085117 (2010).

[25] C.H. Booth, Yu Jiang, D.L. Wang, J.N Mitchell, P.H. Tobash, E.D. Bauer, M.A. Wall, P.G. Allen, D. Sokaras, D. Nordhund, T.-C. Weng, M.A. Torrez and J.L. Sarrao, Proc. Natl. Acad. Sci. **109**, 10205 (2012).

[26] A.V. Mirmelstein, E.S. Clementyev, O.V. Kerbel, JETP Letters 90, 485 (2009).

[27] J. Kolorenc, A.B.Shick, L Havela and A.I. Lichtenstein, MRS Proceedings 1264, 1264_Z09-02 (2010). J. Kolerenc et al, MRS Spring Meeting, San Francisco, CA, 2010.

[28] R.S. Mulliken, Ann. Rev. Phys. Chem. **29**, 1 (1978).

[29] N. W. Ashcroft and N.D. Mermin, "Solid State Physics," Holt Rinehart and Winston, New York, 1976.

[30] A. Mirmelstein and M. Ryzhkov, Reports on the results of Contract B590089; J. G. Tobin, M. Ryzhkov, A. Mirmelstein, "Contract B590089: Technical Evaluation of the Pu Cluster Calculations," LLNL-TR-516874, LLNL, Livermore, CA, USA, 2011.

Table 1

Individual and average configurations for all non-equivalent sites in the Pu_{19} crystal fragment and isolated particle calculated with both the standard extended and truncated basis sets.

Object	Standard basis set	Truncated basis set
Pu_{19} crystal cluster	Data from Ref. [1]	
Pu1 (one central atom)	$5f^{5.48}6d^{3.22}7s^{0.08}7p^{-0.54}$	$5f^{5.30}6d^{2.15}7s^{0.57}7p^{-0.12}$
Pu2 (12 neighbors of Pu1)	$5f^{5.55}6d^{1.96}7s^{0.43}7p^{0.23}$	$5f^{5.59}6d^{1.47}7s^{0.79}7p^{0.11}$
Pu3 (6 next neighbors of Pu1)	$5f^{5.91}6d^{0.97}7s^{0.59}7p^{0.16}$	$5f^{6.23}6d^{1.22}7s^{0.55}7p^{0.08}$
Average configuration	$\mathbf{5f^{5.66}6d^{1.71}7s^{0.46}7p^{0.17}}$	$\mathbf{5f^{5.78}6d^{1.43}7s^{0.70}7p^{0.09}}$
Pu_{19} isolated particle		
Pu1 (one central atom)	$5f^{5.43}6d^{3.38}7s^{-0.10}7p^{-1.02}$	$5f^{5.22}6d^{2.64}7s^{0.46}7p^{0.17}$
Pu2 (12 neighbors of Pu1)	$5f^{5.50}6d^{2.31}7s^{0.33}7p^{0.09}$	$5f^{5.23}6d^{2.05}7s^{0.67}7p^{0.18}$
Pu3 (6 next neighbors of Pu1)	$5f^{5.65}6d^{1.30}7s^{0.52}7p^{0.12}$	$5f^{5.31}6d^{1.41}7s^{0.83}7p^{0.12}$
Average configuration*	$\mathbf{5f^{5.54}6d^{2.05}7s^{0.37}7p^{0.04}}$	$\mathbf{5f^{5.25}6d^{1.88}7s^{0.71}7p^{0.16}}$
* (Total number of valence electrons is 8.0)		

Table 2

Individual and average configurations for all non-equivalent sites in the Pu_{79} crystal fragment and isolated particle calculated with the standard extended basis (crystal fragment, [1]) and truncated basis set (systems of both geometries).

Object	Crystal fragment		Isolated particle
	Extended basis set	**Truncated basis set**	**Truncated basis set**
Pu_{79}	Data from Ref. [1]		
Pu1 (one central atom)	$5f^{5.51}6d^{2.67}7s^{0.30}7p^{-0.23}$	$5f^{5.26}6d^{1.98}7s^{0.75}7p^{0.22}$	$5f^{5.19}6d^{1.81}7s^{0.62}7p^{0.19}$
Pu2 (12 neighbors of central atom)	$5f^{5.51}6d^{2.85}7s^{0.22}7p^{-0.27}$	$5f^{5.20}6d^{2.12}7s^{0.73}7p^{0.16}$	$5f^{5.21}6d^{2.28}7s^{0.63}7p^{0.20}$
Pu3 (6 next neighbors of central atom)	$5f^{5.48}6d^{2.96}7s^{0.19}7p^{-0.12}$	$5f^{5.18}6d^{2.25}7s^{0.70}7p^{0.11}$	$5f^{5.33}6d^{2.61}7s^{0.64}7p^{0.16}$
Pu4 (24 atoms of next coord. sphere)	$5f^{5.90}6d^{2.50}7s^{0.41}7p^{0.17}$	$5f^{6.17}6d^{1.95}7s^{0.72}7p^{0.14}$	$5f^{5.46}6d^{2.26}7s^{0.61}7p^{0.11}$
Pu5 (12 atoms of next coord. sphere)	$5f^{5.14}6d^{1.87}7s^{0.47}7p^{0.31}$	$5f^{5.86}6d^{1.46}7s^{0.65}7p^{0.16}$	$5f^{5.03}6d^{1.83}7s^{0.58}7p^{0.08}$
Pu6 (24 atoms of next coord. sphere)	$5f^{4.72}6d^{1.40}7s^{0.45}7p^{0.28}$	$5f^{4.95}6d^{1.10}7s^{0.58}7p^{0.14}$	$5f^{4.99}6d^{1.77}7s^{0.61}7p^{0.09}$
Average configuration*	$\mathbf{5f^{5.33}6d^{2.16}7s^{0.38}7p^{0.13}}$	$\mathbf{5f^{5.52}6d^{1.67}7s^{0.67}7p^{0.14}}$	$\mathbf{5f^{5.20}6d^{2.07}7s^{0.61}7p^{0.12}}$
* (Total number of valence electrons is 8.0)			

Figure Captions

Figure 1 The structures of δ-Pu-like Pu_{19}, Pu_{79}, and Pu_{201} crystal clusters are shown here. The Pu_{79} and Pu_{201} clusters contains a Pu_{19} cluster as a "core" (showed as the dark spheres). Pu1 is the central atom of the Pu_{19} cluster: twelve Pu2 and six Pu3 atoms form its nearest neighbors and the next nearest neighbors, respectively.

Figure 2 Total and partial densities of states (DOS) for the central Pu1 atom of a Pu_{19} crystal cluster (left) and of a Pu_{19} isolated particle (right) calculated using truncated basis sets. Dashed lines correspond to $p_{1/2}$, $d_{3/2}$, and $f_{5/2}$ DOS, solid lines correspond to $p_{3/2}$, $d_{5/2}$, and $f_{7/2}$ DOS (the vertical solid line at zero energy corresponds to the Fermi and separates the occupied and the vacant states). Calculations were performed with truncated basis functions the use of which significantly suppresses the unphysical negative values of 7p partial DOS as compared to the standard extended basis set. Please see the text for detailed explanation.

Figure 3 Total and partial densities of states (DOS) for the central Pu1 atom of a Pu_{79} crystal cluster (left) and of a Pu_{79} isolated particle (right). Dashed lines correspond to $p_{1/2}$, $d_{3/2}$,and $f_{5/2}$ DOS, solid lines correspond to $p_{3/2}$, $d_{5/2}$,and $f_{7/2}$ DOS. Calculations were performed using truncated basis sets. Calculations were performed with truncated basis functions the use of which significantly suppresses the unphysical negative values of 7p partial DOS as compared to the standard extended basis set. Please see the text for detailed explanation.

Figure 4 Partial Pu6s densities of states (DOS) for the three types of non-equivalent sites in Pu_{19} crystal cluster (left) and Pu_{19} free-standing particle (right). Solid lines show DOS for the Pu1 site (the only site in a cluster), broken lines show the contribution

form twelve Pu2 sites, and dashed lines correspond to the contributions due to six Pu3 sites. The height of each contribution corresponds to the number of equivalent sites in a cluster.

Figure 5 Partial Pu6s density of states (DOS) for the six types of non-equivalent sites in Pu_{79} crystal cluster (left) and Pu_{79} free-standing particle (right). Solid lines show contributions from Pu1, Pu3, and Pu5 sites, whereas the contributions from Pu2, Pu4, and Pu6 sites are shown by broken lines.

Figure 6 Partial Pu4f densities of states (DOS) for non-equivalent sites in the Pu_{19} and Pu_{79} crystal clusters and isolated particles. Calculations were performed using the truncated basis functions. For Pu_{19} systems solid lines show the contributions from Pu1 site, broken lines correspond to the contributions from Pu2 sites, and dashed lines – from Pu3 sites. For Pu_{79} systems solid lines show the contributions due to Pu1, Pu3, and Pu5 sites, whereas the contributions due to Pu2, Pu4, and Pu6 are shown by dashed lines. The lowest panel reproduces the experimentally measured Pu4f core level photoemission spectra recorded from a large crystallite δ-Pu sample and a polycrystalline α-Pu sample [2]. Note the different energy scales for the calculated (top scale) and experimental (bottom scale) spectra.

Figure 7 Total and partial densities of states (DOS) for the central Pu1 atom of a Pu_{19} crystal cluster (left) and of a Pu_{19} isolated particle (right) calculated using standard extended basis sets. The sums of DOS for $7p_{1/2}$ and $7p_{3/2}$, $6d_{3/2}$ and $6d_{5/2}$, $5f_{5/2}$ and $5f_{7/2}$ states are shown. The unphysical negative values of 7p partial DOS are due to the use of diffuse basis functions. Please see Figure 2 for a comparison and the text for detailed explanation.

Figure 8 Total and partial densities of states (DOS) for the central Pu1 atom of a Pu_{201} crystal cluster. Dashed lines correspond to $p_{1/2}$, $d_{3/2}$, and $f_{5/2}$ DOS, solid lines show the DOS for the $p_{3/2}$, $d_{5/2}$, and $f_{7/2}$ states.

Figure 9 The summary of total densities of states (DOS) for the central Pu1 atom for Pu clusters and nanoparticles of different size calculated using truncated basis sets. The upper panel shows the electronic density of states of metallic plutonium obtained at photon energy 125 eV (on resonance) by Resonance Photoemission Spectroscopy (RESPES) technique [2]. The Pu sample was alpha with a delta-like reconstruction on the surface. No energy scale adjustments were applied to calculated or experimental data.

Figure 10 The summary plot of the average Pu5f occupation from Tables 1 and 2 as a function of system size obtained in the present and previous [1] works. The abscissa is given by the cube root of the number of atoms ($\sqrt[3]{N}$) in the structure. For an atom with N = 1, $\sqrt[3]{N} = 1$; for a dimer with N = 2, $\sqrt[3]{N} = 1.26$; for Pu_{19} cluster with N = 19, $\sqrt[3]{N} = 2.67$; for a Pu_{79} cluster with N = 79, $\sqrt[3]{N} = 4.2$; for a Pu_{201} cluster with N=201, $\sqrt[3]{N} = 5.86$. Lines show the size dependences for each set of assumptions used in the RDV cluster calculations, such as cluster structure (crystal fragments and isolated nanoparticles) and the type of basis functions (standard extended and truncated basis sets). The shaded yellow box illustrates the original linear region of Reference 1.

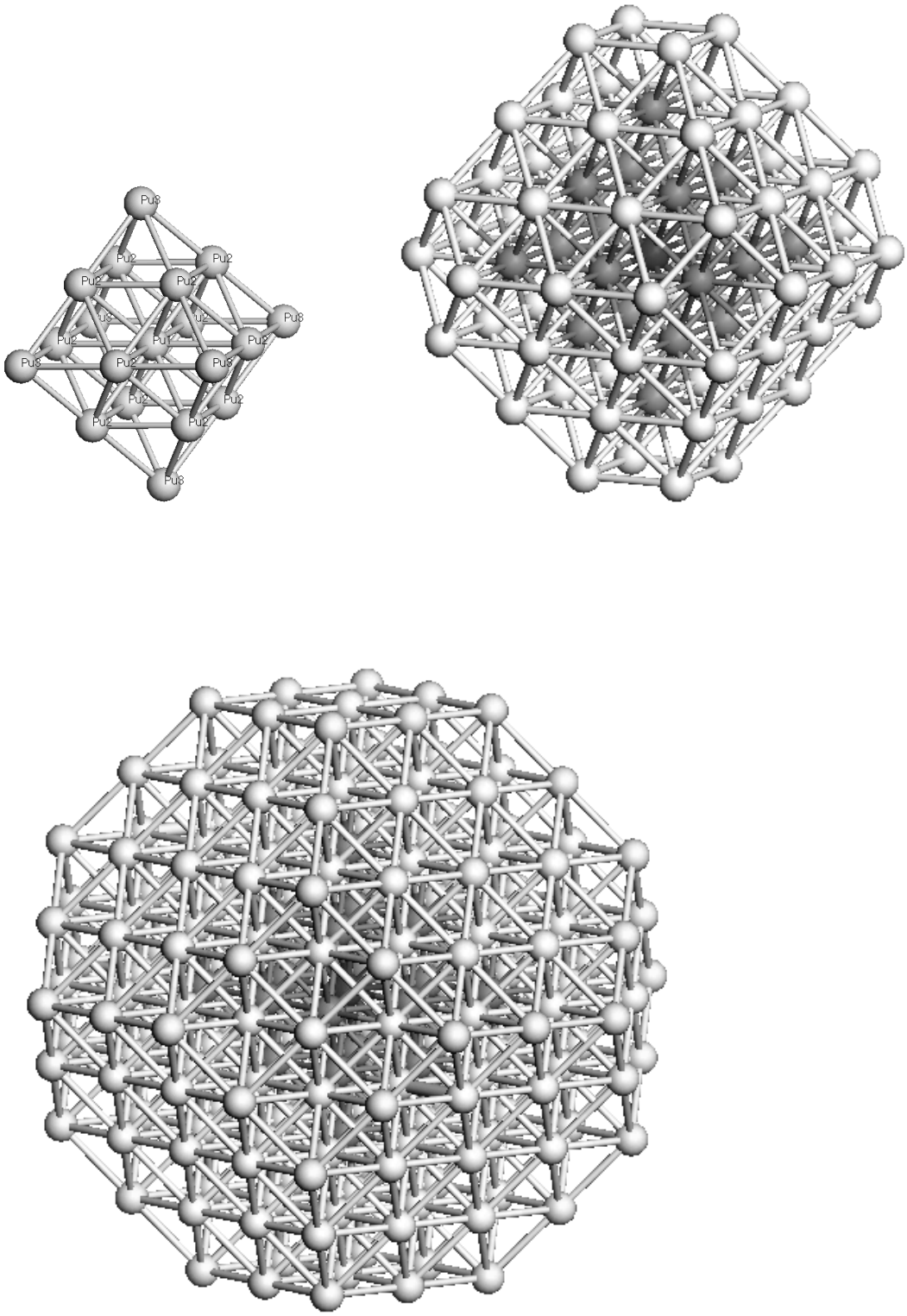

Figure 1

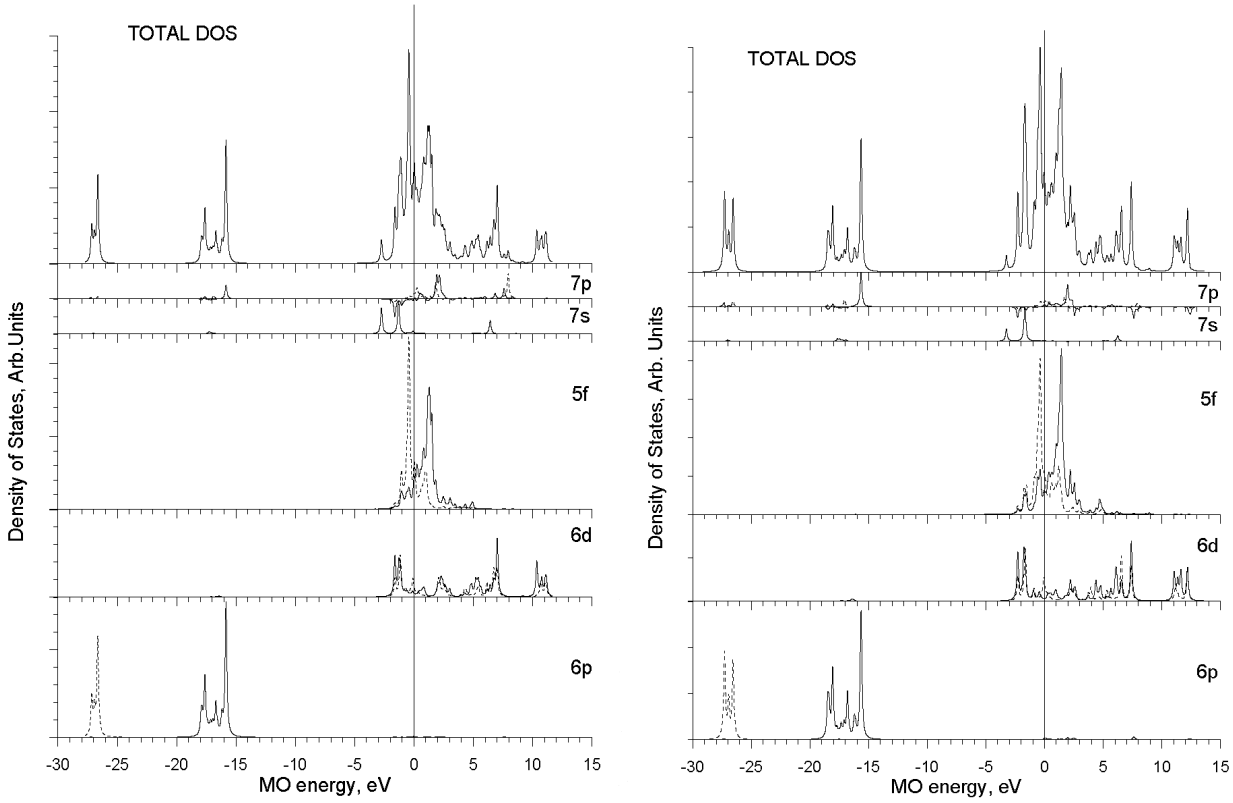
TOTAL DOS
7p
7s
5f
6d
6p
Density of States, Arb.Units
-30 -25 -20 -15 -10 -5 0 5 10 15
MO energy, eV
Pu1 of Pu19 Cluster
TOTAL DOS
7p
7s
5f
6d
6p
Density of States, Arb. Units
-30 -25 -20 -15 -10 -5 0 5 10 15
MO energy, eV
Pu1 of Pu19 Isolated Particle

Figure 2

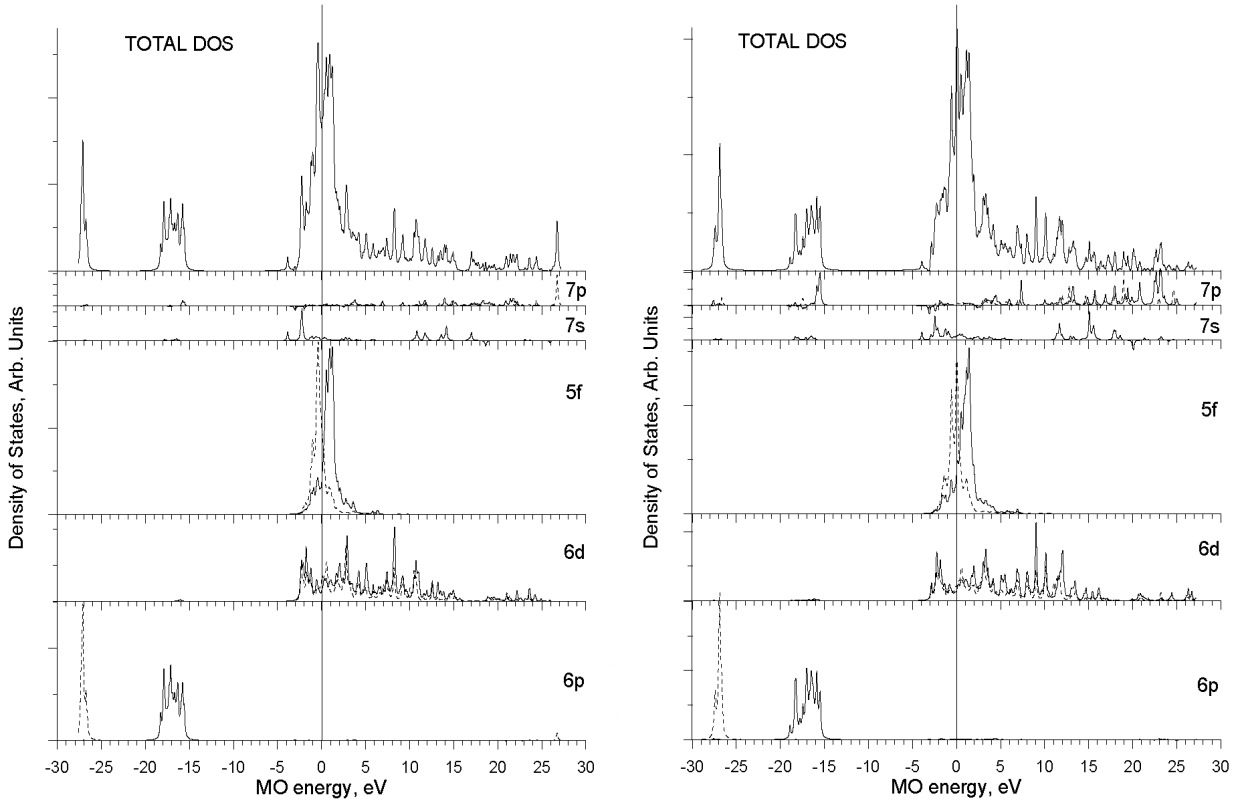

Pu1 of Pu_{79} Cluster **Pu1 of Pu_{79} Isolated Particle**

Figure 3

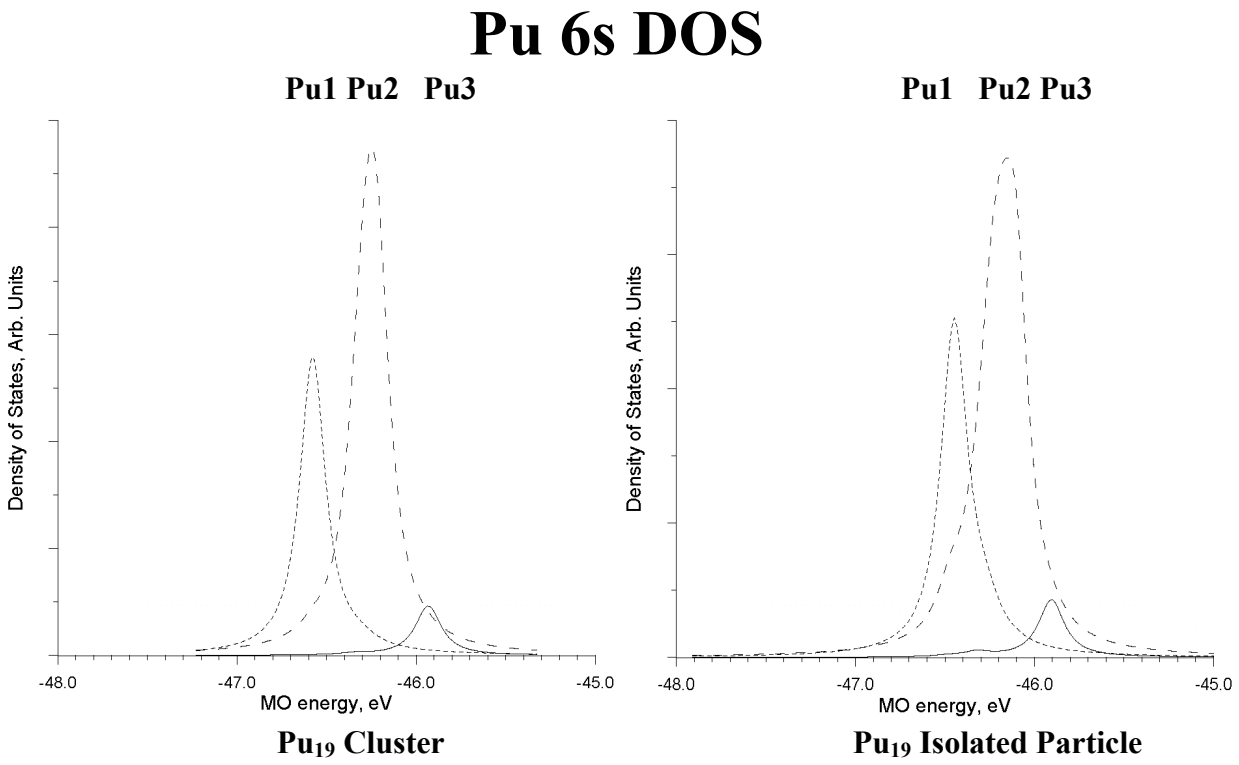
Pu 6s DOS
Pu1 Pu2 Pu3
Density of States, Arb. Units
-48.0
-47.0
-46.0
-45.0
MO energy, eV
Pu19 Cluster
Pu1 Pu2 Pu3
Density of States, Arb. Units
-48.0
-47.0
-46.0
-45.0
MO energy, eV
Pu19 Isolated Particle

Figure 4

Pu 6s DOS

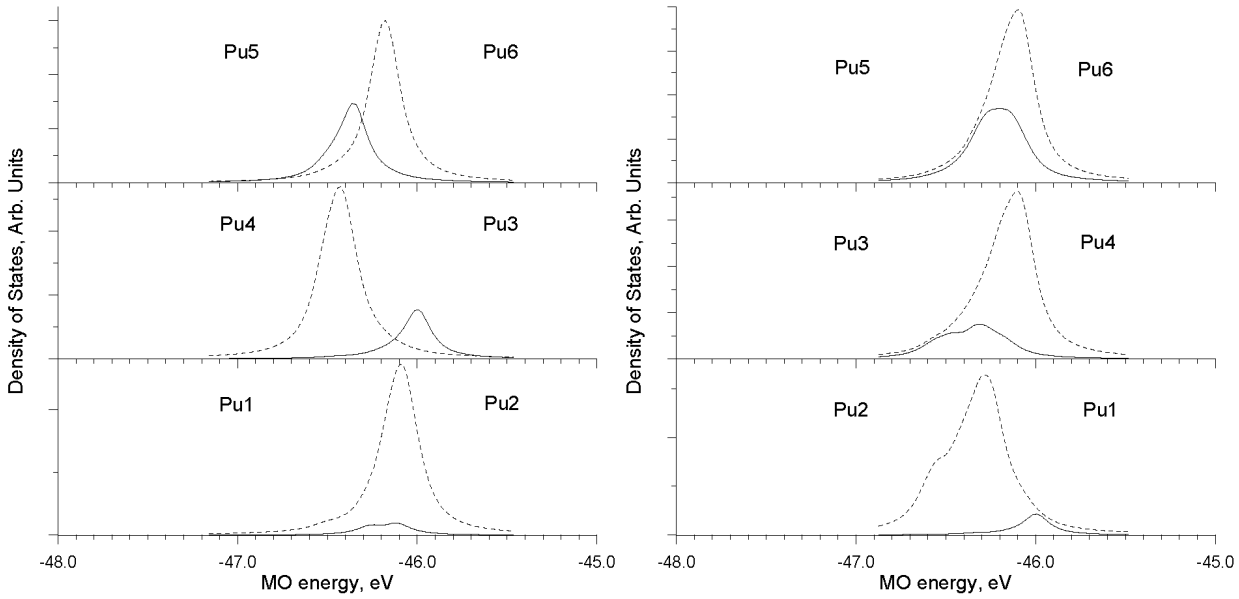

Pu_{19} Cluster **Pu_{19} Isolated Particle**

Figure 5

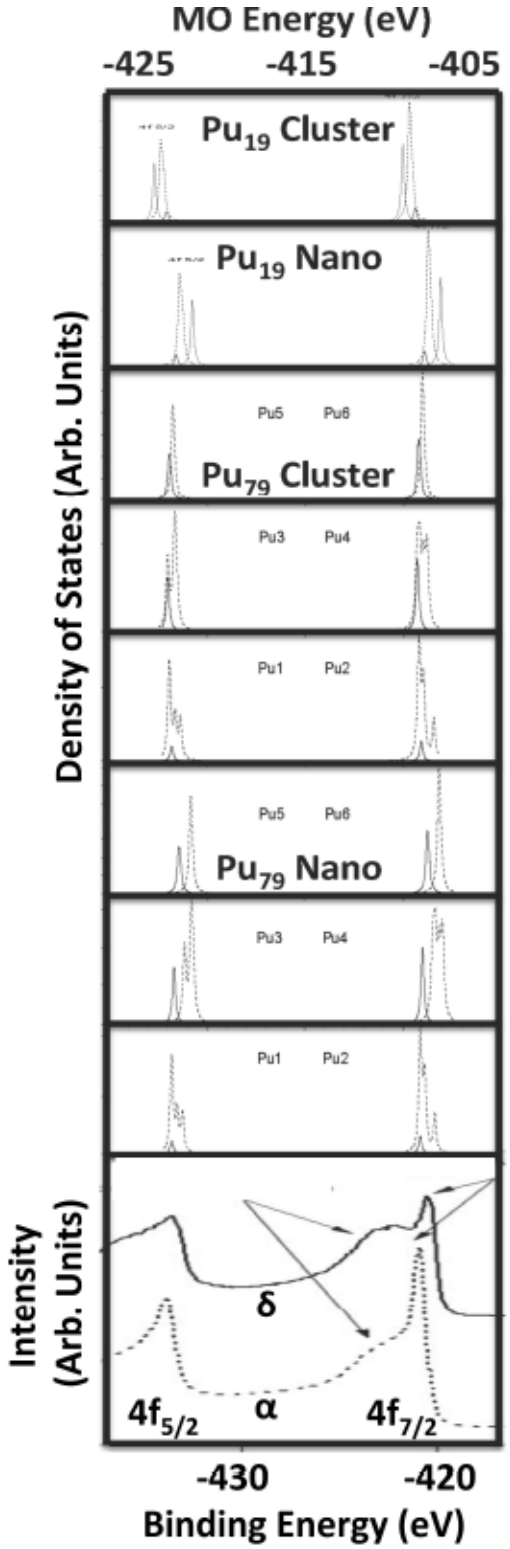
MO Energy (eV)
-425
-415
-405
Pu19 Cluster
Pu19 Nano
Pu5
Pu6
Pu79 Cluster
Pu3
Pu4
Pu1
Pu2
Pu5
Pu6
Pu79 Nano
Pu3
Pu4
Pu1
Pu2
Density of States (Arb. Units)
Intensity (Arb. Units)
δ
α
4f5/2
4f7/2
-430
-420
Binding Energy (eV)

Figure 6

Extended Basis Sets

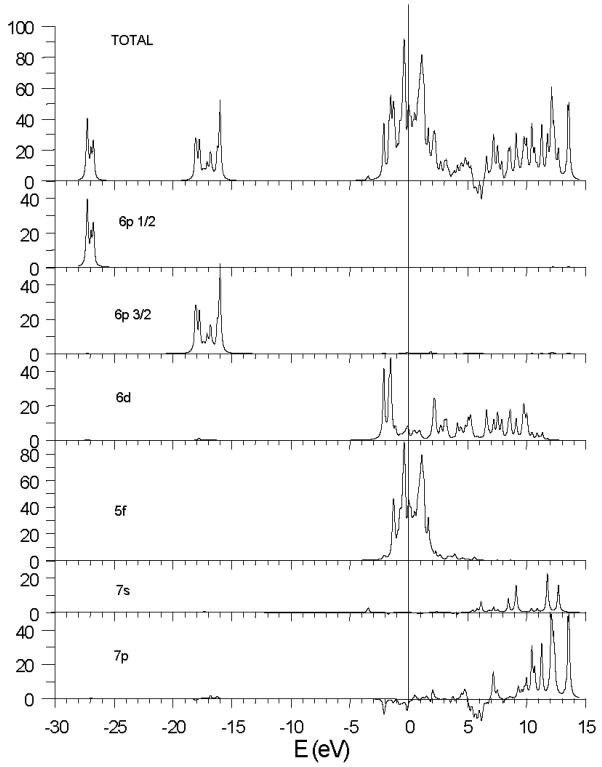

Pu1 of Pu_{19} Cluster

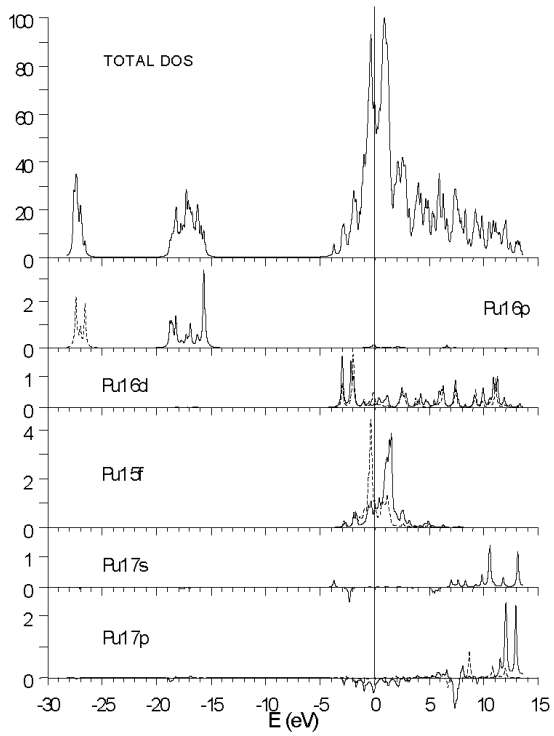

Pu1 of Pu_{19} Isolated Particle

Figure 7

Pu_{201} Cluster

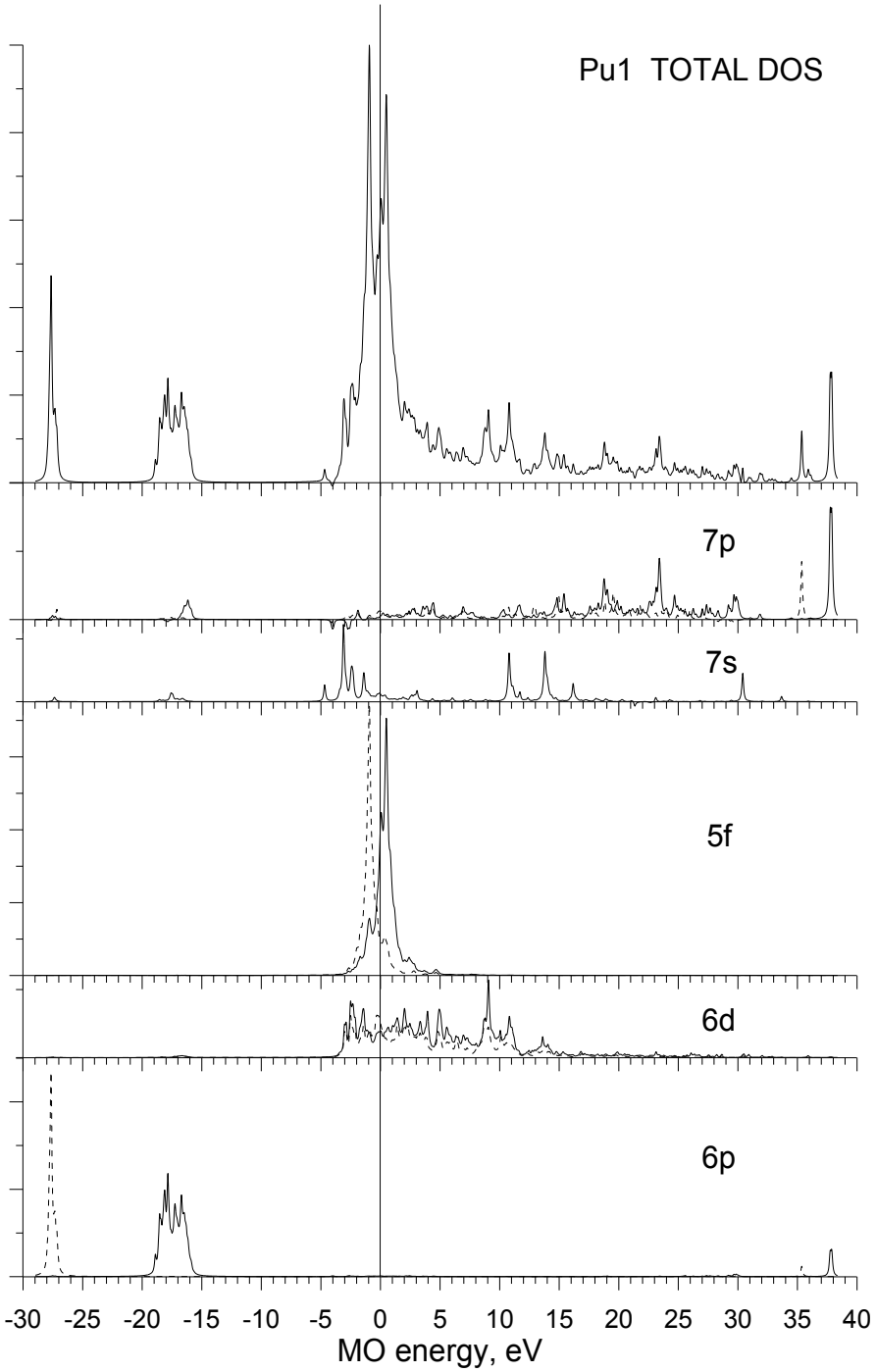

Figure 8

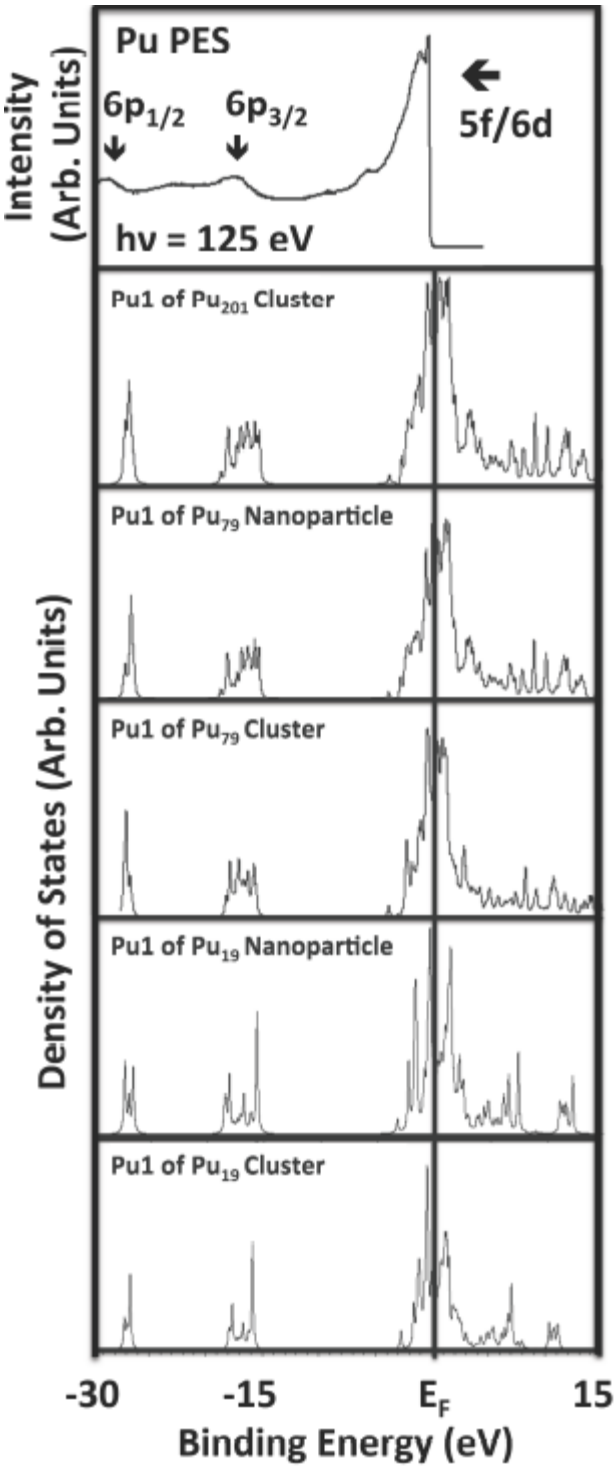
Pu PES
6p1/2
6p3/2
5f/6d
hν = 125 eV
Intensity (Arb. Units)
Pu1 of Pu201 Cluster
Pu1 of Pu79 Nanoparticle
Pu1 of Pu79 Cluster
Pu1 of Pu19 Nanoparticle
Pu1 of Pu19 Cluster
Density of States (Arb. Units)
-30
-15
EF
15
Binding Energy (eV)

Figure 9

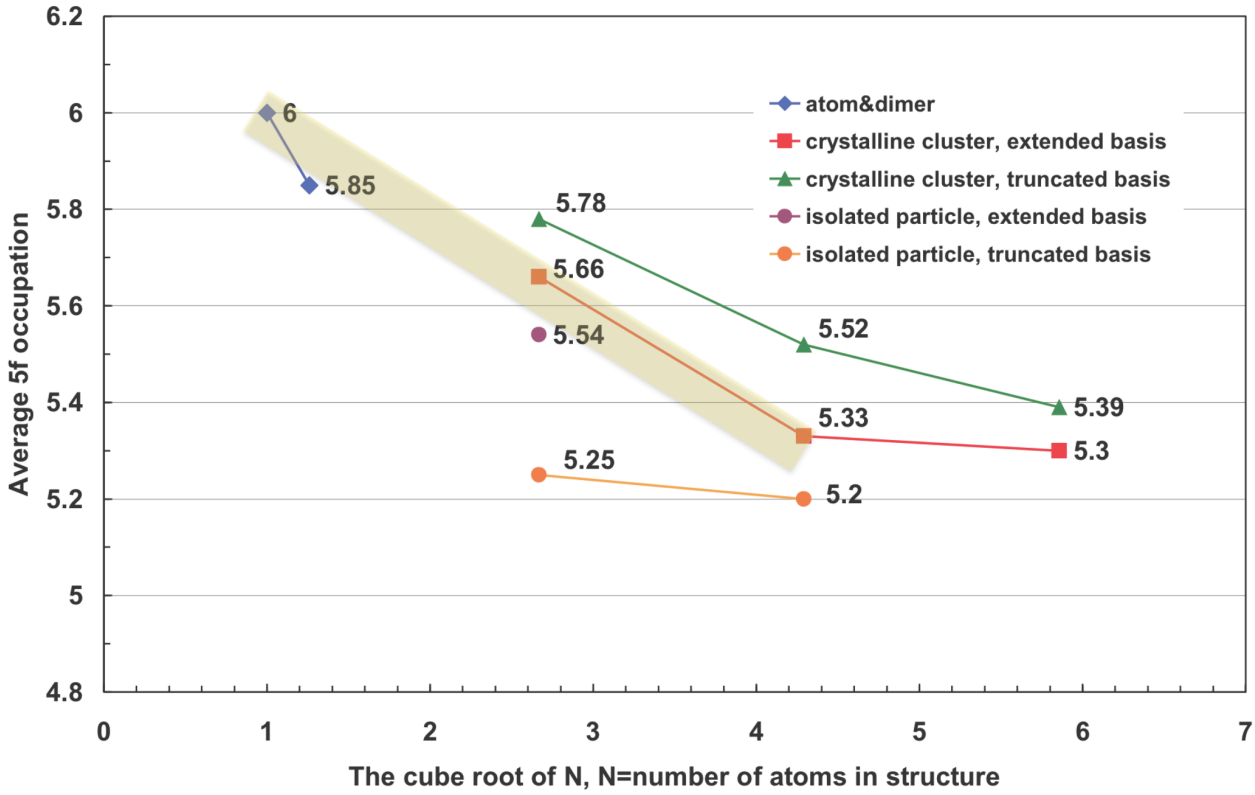
6.2
6
5.8
5.6
5.4
5.2
5
4.8
Average 5f occupation
0
1
2
3
4
5
6
7
The cube root of N, N=number of atoms in structure
atom&dimer
crystalline cluster, extended basis
crystalline cluster, truncated basis
isolated particle, extended basis
isolated particle, truncated basis
6
5.85
5.78
5.66
5.54
5.52
5.39
5.33
5.3
5.25
5.2

Figure 10